Article

Methodology for artificial microswimming using magnetic actuation

Ghanbari, Ali, Bahrami, Mohsen and Nobari, Mohammad R. H.

Ghanbari, Ali ORCID: 0000-0003-1087-8426, Bahrami, Mohsen and Nobari, Mohammad R. H. (2011) Methodology for artificial microswimming using magnetic actuation. Physical Review E (PRE), 83 (4). 046301. ISSN 2470-0045

It is advisable to refer to the publisher's version if you intend to cite from the work.
http://dx.doi.org/10.1103/PhysRevE.83.046301

Methodology for artificial microswimming using magnetic actuation

A. Ghanbari, M. Bahrami,* and M. R. H. Nobari
Mechanical Engineering Department, Amirkabir University of Technology, Tehran, Iran
(Received 31 August 2010; revised manuscript received 15 December 2010; published 1 April 2011)

We propose a methodology for swimming at low-Reynolds-number flows based on ciliary motion of a microswimmer using magnetic actuation of artificial cilia. By solving the coupled magnetic-elastic-hydrodynamic problem, we demonstrate nonreciprocal effective and recovery strokes for cilia that nicely mimic natural cilia beating. Cilia drag forces, microswimmer net displacement, velocity, and efficiency are calculated, and we show the model can swim using a prespecified magnetic actuation. The proposed methodology can be used for devising biomedical microdevices that swim in viscous flows inside the human body.

DOI: 10.1103/PhysRevE.83.046301 PACS number(s): 47.61.−k, 47.63.mf, 47.15.G−

I. INTRODUCTION

Swimming microrobots and nanorobots have attracted considerable attention, owing to their wide applications in biomedicine, such as highly localized drug delivery and minimally invasive surgery [1–4]. Since motion is slow and sizes are small at the microscale level, the Reynolds (Re) number is very small for microswimmers. In such flows, viscous forces play the key role, and swimming methodologies that rely on inertial effect are not applicable [5,6]. Since the inertial effect vanishes at the microscale level, microorganisms and artificial swimmers have a nonreciprocal motion to achieve net displacement.

Microorganisms, in their natural environment, swim using flagellar and/or ciliary motions with a velocity of a few hundreds of micrometers per second, which yields a Re number of the order 10^{-4} [5]. Flagellar motion implies cell propulsion by bending and rotating the flagella protruding from the cell body, respectively, in eukaryotes and prokaryotes. Inspired by flagellar propulsion mechanism of biological cells, swimming microrobots have been developed for swimming at very viscous flows [7–9]. For microrobot propulsion, flagella can be stimulated in different ways; however, magnetic actuation is the most powerful remote method that is utilized for rotating and wiggling the artificial flagella [9,10]. Magnetized filaments that mimic flagella can be fabricated out of a variety of materials with different methods [11]. Although flagellar motion is a practical methodology of drag-based swimming, low efficiency is the main drawback.

Although ciliary motion is widespread in nature, its potential for microscopic artificial swimmers has not yet been realized. Here we propose an efficient microswimmer that uses artificial cilia beating to overcome fluid drag and to propel its spherical body. As in microorganisms, a higher efficiency is expected for ciliary swimming than for flagellar motion [5]. We tune the magnetic field to actuate cilia and create a nonreciprocating configuration, which forms a time-reversal asymmetry required to produce a net displacement in a low-Re-number flow. We solve the coupled magnetic-elastic-hydrodynamic problem to analyze the microswimmer dynamics.

Magnetic actuation of cilia provides strength in wireless energy transmission; moreover, accessibility to magnetic-field-generation equipment (such as magnetic-resonance-imaging systems [12]) can help to implement the method. Recently, magnetically actuated artificial cilia have been devised for fluid transport [13–17]. In this paper, we generate a cilia beat that is completely asymmetric. Our approach can provide a better way to break the time-reversal symmetry and is different than those used by researchers for fluid mixing and propulsion [15–17]. We find the way to produce instability within the cilia, which is required for large bending of cilia.

The swimmer that we are proposing is schematically depicted in Fig. 1 and is composed of a spherical body with radius R, to which two cilia of the length L are attached. To increase the body swimming velocity, the number of cilia can be increased to N. Cilia beat in plane and propel the whole system in fluid with viscosity of μ. A cilia beat cycle is divided into two parts as below:

(a) Effective stroke, in which cilia are straight and strike on the fluid, causing the microswimmer propulsion.

(b) Recovery stroke, in which cilia are bent and move tangentially to their centerlines, therefore creating minimum resistance against the fluid.

Hydrodynamics of low-Re-number flows is governed by Stokes equation for the velocity field $\mathbf{u}$, which is derived from the Navier-Stokes equation by ignoring inertial terms:

$$\nabla p = \mu \nabla^2 \mathbf{u}, \tag{1}$$

$$\nabla \cdot \mathbf{u} = 0, \tag{2}$$

where p is the pressure field and Eq. (2) satisfies the incompressibility of the fluid.

II. MAGNETIC ACTUATION MODELING

Artificial cilia are polymer nanostructures of about 10 μm long, which can be magnetized by incorporating nanoparticles. By molding composite polymers with scattered iron oxide nanoparticles into a template and dissolving the template, an array of magnetized nanorods can be fabricated [18,19]. By actuating the permanently magnetic or superparamagnetic films under an external fixed or rotating magnetic field, the magnetized nanorods mimic natural cilia in order to generate an asymmetric beating. As in typical experiments, here we consider the case where spherical magnetic nanoparticles of radius r_m are implemented over a portion of the length L_m

*Corresponding author: mbahrami@aut.ac.ir

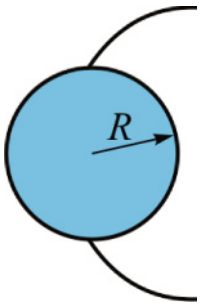

FIG. 1. (Color online) Microswimmer schematic, showing two artificial cilia attached to a spherical body.

of cilia, while distributed uniformly and attached together (Fig. 2).

A cilium is considered as an inextensible cylindrical filament with radius a and length L. Centerline of the cilium is a curve parameterized by its arc-length parameter, s. Tangent to the cilia curve, at a point s on the curve and time t, makes an angle $\alpha(s,t)$ with the horizontal axis. Since cilia are excited under magnetic fields that are spatially homogenous, just magnetic torque is exerted on the filaments and no magnetic force is present. Magnetic torque is calculated through vector product of magnetization (**m**) and magnetic induction (**B**). An external applied magnetic field and one due to the interactions between nanoparticles contribute to the particles magnetization. Tangential and normal components of magnetization can be obtained from [20]

$$m_T = \frac{\frac{4}{3}\pi r_m^3 \chi_T B_T}{\mu_0(1-\chi_T/.6)}, \tag{3}$$

$$m_N = \frac{\frac{4}{3}\pi r_m^3 \chi_N B_N}{\mu_0(1+\chi_N/.12)}, \tag{4}$$

where χ_T and χ_N are susceptibilities in tangential and normal directions, for accounting shape anisotropy. Tangential and normal components of the external magnetic field are denoted by B_T and B_N. Then from the cross product of magnetization and the magnetic field, one can compute the torque per unit length of cilia as

$$M_B = \frac{\pi r_m^2 |\mathbf{B}|^2}{3\mu_0}\left(\frac{\chi_T - \chi_N + \chi_T\chi_N/.4}{(1-\chi_T/.6)(1+\chi_N/.12)}\right) \times \sin 2(\psi-\alpha), \tag{5}$$

where ψ is the angle between total applied magnetic field and a fixed horizontal axis (Fig. 2). We denote coefficient in Eq. (5) by M_{B_0}. Note that ψ and magnetic field magnitude, besides cilia dimensions, are the main parameters that can be properly designed to generate an asymmetrical beat cycle.

III. HYDRODYNAMICS MODELING

The microswimmer force and velocity are necessary parameters to study the dynamics of the swimmer. Since inertial forces are negligible, velocity of the microswimmer is obtained from equation of conservation of linear momentum in the horizontal direction. Forces acting on microrobot body are the following:

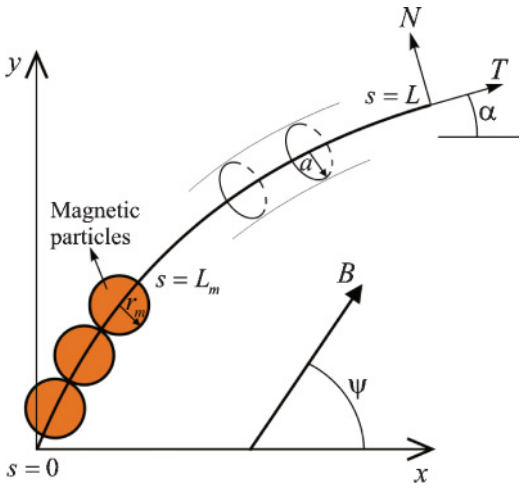

FIG. 2. (Color online) Schematic of a paramagnetic cilium, showing local and global coordinate systems as well as conformation (α)and magnetic field (ψ) angles.

(1) The resultant of drag forces exerted from fluid on cilia, $F_{x,\text{cilia}}$.

(2) Hydrodynamic force for the spherical body with radius R that moves with a velocity of U in a viscous flow, which is $6\pi\mu RU$.

Hence, we can obtain the swimmer velocity from

$$U = \frac{\sum F_{x,\text{cilia}}}{6\pi R\mu}, \tag{6}$$

To calculate cilia drag force, resistive-force theory is used in this work to relate cilium local drag forces to the local velocity [21]

$$\phi_T = -C_T V_T, \tag{7}$$

$$\phi_N = -C_N V_N, \tag{8}$$

where ϕ_T and ϕ_N are tangential and normal drag forces and V_T and V_N are local velocities in tangential and normal direction. C_T and C_N are resistance coefficients and can be found from [22]

$$C_T = \frac{8\pi\mu}{-2+4\ln(2q/a)}, \tag{9}$$

$$C_N = \frac{8\pi\mu}{1+2\ln(2q/a)}, \tag{10}$$

where q is an arbitrary value provided that $q/L \ll 1, a/q \ll 1$.

We can write two geometrical equations to relate velocities in tangential and normal directions:

$$\frac{\partial V_N}{\partial s} = \frac{\partial \alpha}{\partial t} - V_T\frac{\partial \alpha}{\partial s}, \tag{11}$$

$$\frac{\partial V_T}{\partial s} = V_N\frac{\partial \alpha}{\partial s}. \tag{12}$$

We use F and M to denote internal force and moment of a cilium. The balance of force and moment for the cilium yields

$$\frac{\partial F_T}{\partial s} - F_N\frac{\partial \alpha}{\partial s} = \phi_T, \tag{13}$$

$$\frac{\partial F_N}{\partial s} + F_T \frac{\partial \alpha}{\partial s} = \phi_N, \tag{14}$$

$$\frac{\partial M}{\partial s} = F_N. \tag{15}$$

Internal moment of cilia is composed of two parts; one comes from elasticity, which is $EI\partial\alpha/\partial s$ for an Euler-Bernoulli beam. E is the modulus of elasticity and I is the second moment of area. The second part is the actuation moment, which is stated in Eq. (5). Using Eq. (15), we can relate the actuation moment to the normal and elastic force as

$$F_N = EI\frac{\partial^2 \alpha}{\partial s^2} + M_B. \tag{16}$$

Using Eqs. (11)–(14), one can eliminate velocity components and obtain the following equations [23]:

$$\frac{\partial^2 F_T}{\partial s^2} = \left(1 + \frac{C_T}{C_N}\right)\frac{\partial F_N}{\partial s}\frac{\partial \alpha}{\partial s} + \frac{C_T}{C_N}F_T\left(\frac{\partial \alpha}{\partial s}\right)^2 + F_N\frac{\partial^2 \alpha}{\partial s^2}, \tag{17}$$

$$\frac{\partial^2 F_N}{\partial s^2} + \left(1 + \frac{C_N}{C_T}\right)\frac{\partial F_T}{\partial s}\frac{\partial \alpha}{\partial s} + F_T\frac{\partial^2 \alpha}{\partial s^2} + C_N\frac{\partial \alpha}{\partial t} = \frac{C_N}{C_T}F_N\left(\frac{\partial \alpha}{\partial s}\right)^2. \tag{18}$$

These equations, along with Eq. (16), form a system of nonlinear partial differential equations, which couples the cilium elastic, hydrodynamic, and magnetic interactions. The magnetic actuation force is inserted into the coupled system as a module and can be easily changed for any different actuation mechanism. It can be seen that although the equations of fluid mechanics in the low-Reynolds-number regime are linear, the instantaneous shape of a cilium over a beat cycle is obtained from solution of a complex coupled nonlinear system. Each cilium is divided into 50 discretized segments. Once the shape of the cilium at time t and the magnetic moment per unit length are known, one can calculate the normal force from Eq. (16). Knowing F_N and α, we solve Eq. (17) for F_T, which is a second-order ordinary differential equation now. Then, we solve Eq. (18) using a Crank-Nicolson finite-difference method to propagate α in time. The method computes α at time $t + dt/2$, and $\alpha(s,t)$ can be obtained from

$$\alpha(s,t+dt) \approx 2\alpha(s,t+dt/2) - \alpha(s,t). \tag{19}$$

Moreover α, drag forces, and local velocities of the cilium can be obtained from the model. Inputs to the model are the initial shape of the cilium and actuation torque for every point of cilium at any time. Finally, equations of motion are written to find dynamic parameters of the swimmer. To take into account all velocities experienced by cilia in Eqs. (7) and (8), we consider the tangential and normal components of body velocity on cilia as $U\cos\alpha$ and $U\sin\alpha$, respectively. A detailed description of the motion equations can be found in the supporting document [24].

IV. NUMERICAL EXAMPLE

As an example, we have solved the system dynamics model for a microswimmer with a body radius of $R = 40\,\mu$m and numerically solved the equations to find cilia drag forces and determine the microswimmer propulsive velocity. A zero-velocity boundary condition in infinity and no-slip boundary conditions at the cilia outer surface are applied. Cilia has modulus of elasticity $E = 5$ GPa, a length of $L = 15\,\mu$m, and a radius of $a = 12.5$ nm, so the slenderness property is satisfied ($a/L \ll 1$). Magnetic nanoparticles have the same diameter as cilia and susceptibilities $\chi_T = 4.5$ and $\chi_N = 1$ in tangential and normal directions. Fluid has a viscosity $\mu = 0.001$ kg/(m · s).

The magnetized length of cilia is considered $L_m = 0.4L$ from where cilia is attached to the body surface ($s = 0$). A segmental magnetization of cilia is the way we generate an instability that causes cilia motion during effective stroke and a large bending in recovery. The instability reduces the energy threshold required for buckling of the filaments. The cilia start beating from $\alpha(s,0) = 150^\circ$. During an effective stroke, a uniform magnetic field of magnitude $|\mathbf{B}| = 70$ mT is applied at an angle$\alpha(0,t) - \pi/4$, which implies that magnetic field is rotated from 105° at first to about −35° in a 14.5-ms time period. This angle geometry maximizes the sine function in Eq. (5), which results in a maximum torque on filaments.

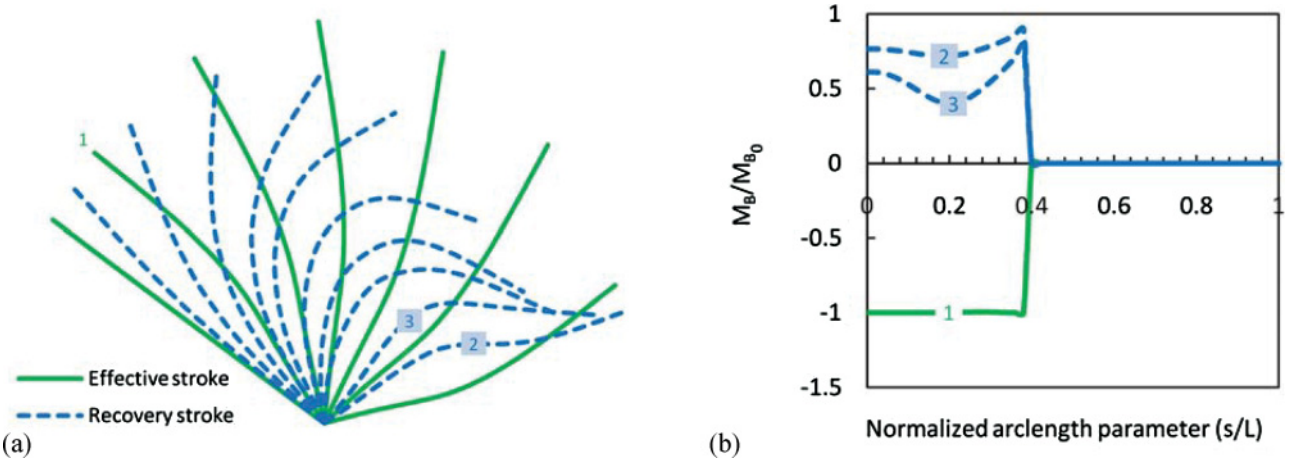

FIG. 3. (Color online) Motion of a cilium actuated by a magnetic field during a beat cycle. (a) Cilium shape for several instants in effective and recovery strokes; (b) normalized magnetic torque distribution along the cilium for three instances.

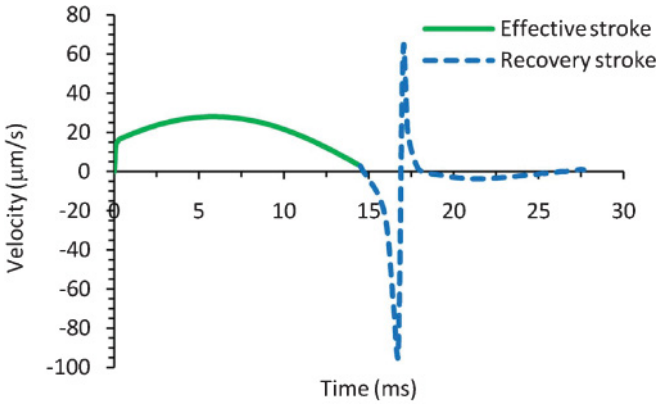

FIG. 4. (Color online) The microswimmer velocity during a beat cycle.

For the recovery stroke, we apply a horizontal constant field of magnitude 90 mT and a sinusoidal transverse field described by $0.7\sin(10t)$ (Tesla) to be applied simultaneously in next 2.5 ms after the end of effective stroke. Then applied fields are removed for next 10.5 ms, when recovery stroke finishes. Using the aforementioned magnetic actuation, it takes 27.5 ms to generate a complete nonreciprocal beat cycle. Cilia beating in fluid under magnetic actuation during a beat cycle is shown in Fig. 3(a). During an effective stroke, magnetic torque remains at almost maximum for all points along a magnetized segment of cilium, which is shown in Fig. 3(b), for instance, 1. Torque distribution for all effective instances is similar to that of instance 1. Magnetic torque shown in Fig. 3(b) for instances 2 and 3 causes a large bending of cilia in recovery stroke, where cilia are required to have a minimal effect on fluid. Then torque is reduced to zero for other remaining instances, and elasticity recovers cilia to the initial shape. Successive effective and recovery cilia strokes produce continuous propulsion for the microswimmer.

Knowing cilia drag forces, from Eq. (6), we can compute the microswimmer propulsive velocity for any instance during the cilia beat cycle (Fig. 4). During an effective stroke, velocity increases with time to a maximum value where cilia are perpendicular to motion direction and then decreases. Switching to the recovery stroke, velocity starts increasing in the reverse direction. When the magnetic field is removed, velocity is reversed due to the fluid velocity and gradually decreases to zero. The area under the curve in Fig. 4 is the artificial-swimmer net displacement. We can also determine the mean swimming velocity by dividing the net displacement by the duration of a beat cycle. Figure 5 shows the mean swimming velocity for different body radii.

To see how the artificial cilia mimic their natural counterparts, we use the model introduced in [23] to regenerate the natural-cilia beat patterns. The model parameters have been obtained by fitting to ciliary beat patterns observed in *Paramecium* by Sleigh [25] under conditions where the beats are two dimensional [23]. We have compared the recovery stroke of the artificial cilia with the data on ciliary beat patterns of *Paramecium*. Figure 6 shows the result under conditions when the beating is two dimensional. It is seen that the patterns are analogous. As well, cilia effective strokes of the both *Paramecium* and the artificial swimmer are very similar.

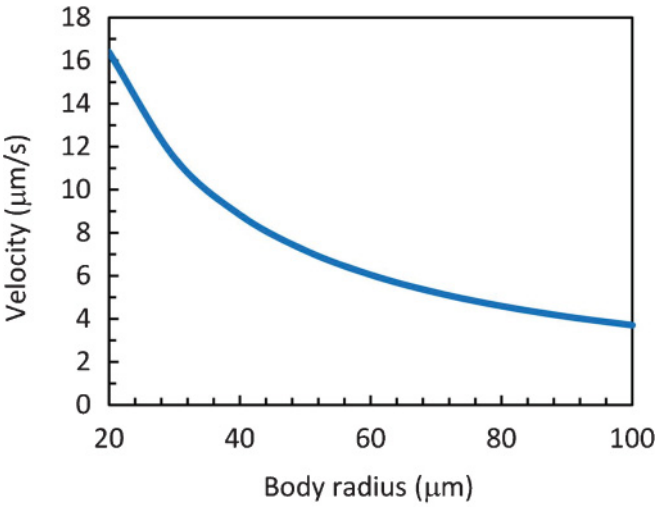

FIG. 5. (Color online) Mean swimming velocity for microswimmers with different body radii.

V. EFFICIENCY

The swimmer propulsive efficiency is defined as the ratio of required energy for propulsion to the mean rate of energy dissipation during a beat cycle, P. The energy for propulsion is quantified with body swimming velocity, U, times the propulsive force, F. The efficiency can be obtained from

$$\eta = \frac{FU}{P}, \tag{20}$$

where P for one cilium can be expressed by

$$P = \int_0^L (\phi.V)ds. \tag{21}$$

Since in the recovery stroke the body velocity does not accord to the propulsion direction, the output energy during this interval should be subtracted from the one for the effective stroke. The proposed microswimmer has an efficiency of 0.000 295 obtained by the above method. In order to explore the effect of cilia beat pattern on the swimmer's velocity and efficiency, we have calculated swimming velocities and efficiencies when cilia beat with different patterns shown in Fig. 7 during the recovery stroke; the effective stroke is similar to that shown in Fig. 3(a). The swimmer velocity

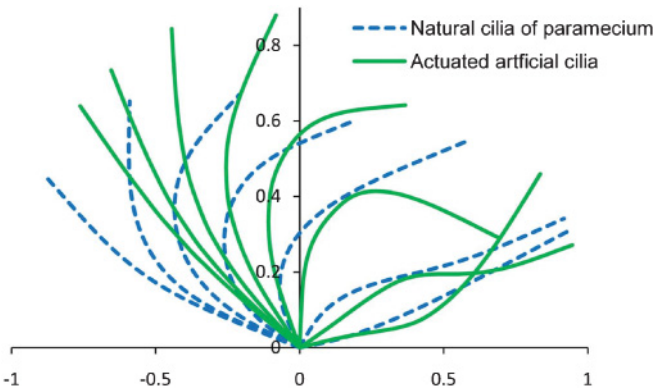

FIG. 6. (Color online) Comparison between artificial- and natural-cilia shapes during recovery strokes.

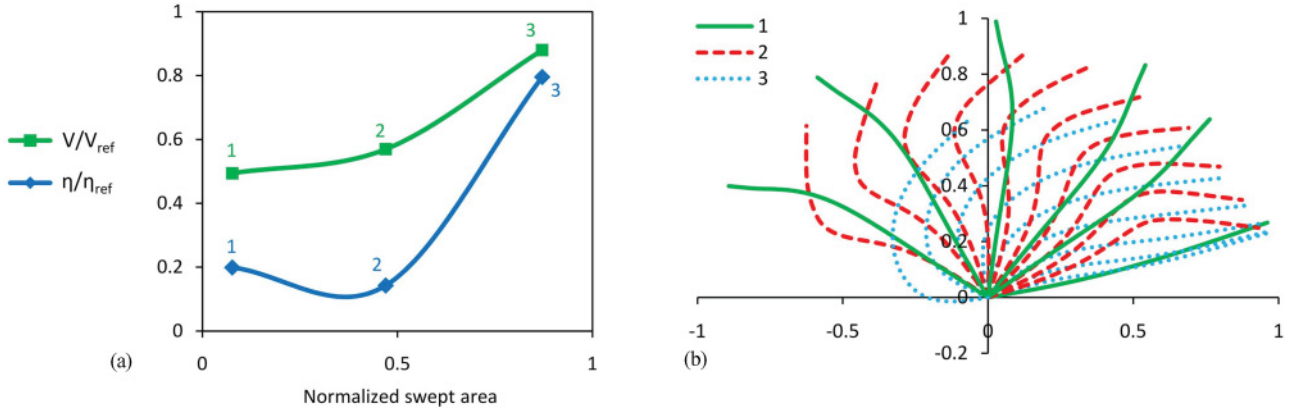

FIG. 7. (Color online) (a) Microswimmer velocity and efficiency vs normalized swept area for (b) different cilia recovery patterns 1, 2, and 3.

and efficiency, normalized by their values obtained for the prescribed magnetic actuation as a reference, V_{ref} and η_{ref}, are drawn in Fig. 7 for recovery beatings 1, 2, and 3 versus normalized swept area (the area difference swept by cilia in effective and recovery strokes).

We found that the swimming velocity is not a linear function of swept area, as we see for flow rate in fluid propulsion [14], and thus the swept area or the net fluid flow is not an appropriate measurement of efficiency. When cilia move close to the body surface, the swept area is increased; however, they should beat more tangentially to their centerlines to produce a higher velocity and efficiency for the microswimmer. From Fig. 7, one can see that a higher efficiency does not guarantee a higher velocity. The optimization can be carried out with velocity or efficiency as a cost function to determine the most desired cilia beat pattern.

In our proposition for cilia nonreciprocal motion, we assumed magnetic fields to be applied with specific magnitude and direction. We should mention that the model is sensitive to cilia dimensions, and the suggested values should be changed in the case of any change in cilia dimensions. Number of cilia can be increased to N, as restricted by space and fabrication technology, which results in a microswimmer with a higher net displacement and velocity. If we have 500 cilia on each side of microrobot body, it can reach a swimming velocity of 0.11 mm/s and an efficiency of 0.00 412. *Paramecium* utilizes rows of cilia beating with a phase difference between neighboring cilia, creating a wave at the tips, which is called the metachronal wave. This phenomenon has been demonstrated to reduce the energy expenditure during effective and recovery strokes [26,27]. Metachronism does not occur in proposed microswimmer due to an identical phase angle for all cilia, although the artificial swimmer can benefit from increasing cilia number to produce more power and achieve greater velocity and efficiency.

VI. CONCLUSION

In summary, we have introduced an artificial microswimmer that uses magnetic actuation to generate a nonreciprocal cilia motion for propulsion. Solving the complex coupled magnetic-elastic-hydrodynamic problem, we have calculated the swimming velocity of the microrobot in low-Re-number flows. The swimming methodology, which should be explored more and put to the test, shows a promising future and provides a reasonable velocity. The proposed magnetic actuation of cilia causes a beating configuration that nicely mimic natural cilia of *Paramecium*. The swimming velocity and efficiency do not show a linear dependence on swept area. The most efficient beat pattern is similar to the one for natural cilia; however, its parameters should be determined through an optimization approach. We found that partial magnetization of the artificial cilia generates a necessary instability that causes a large buckling of cilia during the recovery stroke. The study presented can be used as a methodology for an artificial microswimmer with a desired motion. The most interesting application of this microswimmer is for biomedical tasks inside the human body.

This work is partially supported by Iranian Nanotechnology Initiative (INI).

[1] R. Dreyfus, J. Baudry, M. L. Roper, M. Fermigier, H. A. Stone, and J. Bibette, Nature (London) **437**, 862 (2005).
[2] A. Najafi and R. Golestanian, Phys. Rev. E **69**, 062901 (2004).
[3] B. Behkam and M. Sitti, Trans. ASME, J. Dyn. Syst. Meas. Control **128**, 36 (2006).
[4] A. M. Leshansky, Phys. Rev. E **80**, 051911 (2009).
[5] S. Childress, *Mechanics of Swimming and Flying* (Cambridge University Press, Cambridge, UK, 1981).
[6] T. Uchiyama and K. Kikuyama, J. Micromech. and Microeng. **14**, 1537 (2004).
[7] G. Kosa and M. Shoham, IEEE Trans. Robotics **23**, 137 (2007).
[8] S. E. Spagnolie, Phys. Rev. E **80**, 046323 (2009).
[9] J. Abbott, K. E. Peyer, M. C. Lagomarsino, L. Zhang, L. Dong, J. K. Kaliakatsos, and B. J. Nelson, Int. J. Robotics Res. **28**, 1434 (2009).

[10] K. B. Yesin, K. Vollmers, and B. J. Nelson, Int. J. Robotics Res. **25**, 527 (2006).
[11] L. Zhang, J. J. Abbott, L. X. Dong, B. E. Kratochvil, D. Bell, and B. J. Nelson, App. Phys. Lett. **94**, 064107 (2009).
[12] S. Martel, M. Mohammadi, O. Felfoul, Z. Lu, and P. Pouponneau, Int. J. Robotics Res. **28**, 571 (2009).
[13] V. V. Khatavkar, P. D. Anderson, J. M. J. den Toonder, and H. E. H. Meijer, Phys. Fluids **19**, 083605 (2007).
[14] S. N. Khaderi, M. G. H. M. Baltussen, P. D. Anderson, D. Ioan, J. M. J. den Toonder, and P. R. Onck, Phys. Rev. E **79**, 046304 (2009).
[15] A. R. Shields, B. L. Fiser, B. A. Evans, M. R. Falvo, S. Washburn, and R. Superfine, PNAS **107**, 15670 (2010).
[16] A. Alexeev, J. M. Yeomans, and A. C. Balazc, Langmuir **24**, 12102 (2008).
[17] Y. W. Kim and R. R. Netz, Phys. Rev. Lett. **96**, 158101 (2006).
[18] B. A. Evans, A. R. Shields, R. Lloyd Carroll, S. Washburn, M. R. Falvo, and R. Superfine, Nano Lett. **7**, 1428 (2007).
[19] C. Goubault, P. Jop, M. Fermigier, J. Baudry, E. Bertrand, and J. Bibette, Phys. Rev. Lett. **91**, 260802 (2003).
[20] M. Roper, R. Dreyfus, J. Baudry, M. Fermigier, J. Bibette, and H. A. Stone, J. Fluid Mech. **554**, 167 (2006).
[21] J. Gray and G. Hancock, J. Exp. Biol. **32**, 802 (1955).
[22] C. Brennen and H. Winet, Ann. Rev. Fluid. Mech. **9**, 339 (1977).
[23] S. Gueron and K. Levit-Gurevich, Biophys. J. **74**, 1658 (1998).
[24] See supplemental material at [http://link.aps.org/supplemental/10.1103/PhysRevE.83.046301] for a detailed description of the model and motion equations.
[25] M. A. Sleigh, *Aspects of Cell Motility (22nd Symposium of the Society for Experimental Biology)*, edited by P. L. Miller (Cambridge University Press, Cambridge, 1968), p. 131.
[26] S. Gueron and K. Levit-Gurevich, PNAS **96**, 12240 (1999).
[27] S. Michelin and E. Lauga, Phys. Fluids **22**, 111901 (2010).